ASSOCIAZIONE NAZIONALE ITALIANA DI INGEGNERIA SISMICA
ANIDIS
Italian National Association of Earthquake Engineering

XVIII CONVEGNO ANIDIS
L'ingegneria sismica in Italia
ASCOLI PICENO 2019
15-19 Settembre

A novel OpenSees element with improved friction model for Friction Pendulum System isolators

Virginio Quaglini[a], Emanuele Gandelli[a], Paolo Dubini[b]
[a] *Department Architecture, Built Environment and Construction Engineering, Politecnico di Milano, Piazza Leonardo da Vinci 32, 20133 Milan, Italy*
[b] *EUCENTRE, European Centre for Training and Research in Earthquake Engineering, Via A. Ferrata 1, 27100 Pavia, Italy*

Keywords: Friction Pendulum System, OpenSees, bearing element, friction model

ABSTRACT
The increasing use of sliding bearings with curved surfaces, like the Friction Pendulum System® (FPS), as seismic isolators benefits from the improvement of numerical models able to capture their experimental behavior and enhance the predictive capability of nonlinear response history analyses. Nevertheless, the effective implementation of the static coefficient of friction of FPS isolators in software programs for structural analysis has not yet been achieved, and the use of dynamic friction only is a common practice in design. In this study, a novel element has been formulated in the object-oriented finite element software OpenSees by modifying the standard "SingleFPSimple3d" element to represent the behavior of a FPS isolator comprising one concave sliding surface and a spherical articulation accounting for the static coefficient of friction at the breakaway; other features are the inclusion of the dependency of the dynamic coefficient of friction on the instantaneous values of axial load and slide velocity at the interface, and its degradation due to heating during cyclic motion. The new features of the friction model are verified in a code-to-code comparison. A case study dealing with to a reinforced concrete, moment resisting frame is eventually presented to demonstrate the improved prediction capability of the new FPS element over its standard counterpart.

1 INTRODUCTION

The Friction Pendulum System®, or FPS®, (Zayas et al. 1987, 1990), (Mokha et al. 1991) is one of the most popular isolation hardware worldwide thanks to its inherent simplicity, since it provides the main functions required to the isolation system, namely load bearing capacity, lateral flexibility, energy dissipation and re-centering capability, in a single, compact design. In its basic configuration, e.g. Figure 1, the FPS consists of two concave plates (the sliding plate and the basement) and an articulated slider. The primary sliding surface accommodates the horizontal displacement of the superstructure, while the secondary sliding surface accommodates the rotations between the upper and the lower structural elements. Pads made of low friction thermoplastic materials, like e.g. PolyTetraFluoroEthylene (PTFE), Ultra High Molecular Weight PolyEthylene (UHMWPE) and Polyammide (PA) are commonly used in the sliding surfaces as lining materials. Though improved versions with multiple sliding surfaces have been proposed, like e.g., the Double Curved Surface Slider (Fenz and Constantinou 2006) and the Triple Friction Pendulum (Sarlis et al. 2013), their mechanical behaviour follows the same fundamental principles. The isolation behaviour performance is determined by the number of sliding interfaces, the coefficient of friction and the radius of curvature of sliding surfaces: thanks to the curved shape, the primary surface generates a restoring force that is proportional to the horizontal displacement; during the accommodated sliding motion friction provides energy dissipation, which reduces the displacement demand, but increases the amount of residual displacement.

The coefficient of friction of thermoplastic materials is affected from several factors including the contact pressure, the velocity of sliding, the surface temperature, the roughness of the mating surface, wear and contamination, e.g. (Constantinou et al. 1999), (Campbell et al. 1993), (Dolce et al. 2005), (Quaglini et al. 2009, 2012, 2014). The typical dependency on pressure and

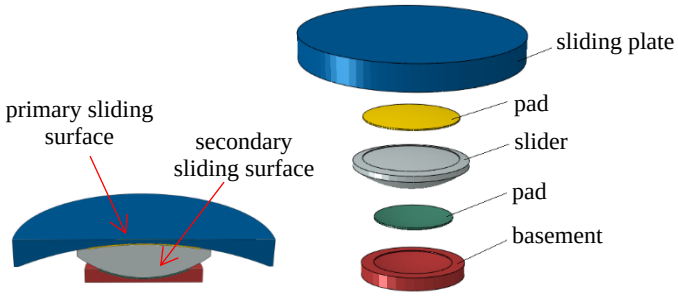

Figure 1. Schematic view of the FPS and its main part

velocity is illustrated in Figure 2. Here μ_{st} denotes the static coefficient of friction developed during sticking between the surfaces, and μ_{dyn} denotes the dynamic coefficient of friction observed during sliding; μ_{dyn} changes with velocity rising from a minimum value μ_{LV} at very low velocity to a maximum steady value μ_{HV} at high speeds. Furthermore, μ_{dyn} decreases during sustained motion, as an effect of the heating of the sliding surface consequent to energy dissipation, e.g. (Constantinou et al. 2007). The drop in the coefficient of friction occurring at the breakaway can be very large: (Constantinou et al. 1990) proposed to assume the ratio between static and low velocity coefficient of friction equal to 4 for unworn PTFE, and similar figures were experimentally derived for other sliding materials, including filled PTFE, UHMWPE and PA, e.g. (Barone et al. 2017), (Quaglini et al. 2012).

The variation of the dynamic coefficient of friction with velocity and pressure was recognized early on as significant and incorporated in software programs for structural analysis such as SAP2000 (CSI 2016), OpenSees (McKenna et al. 2006) and 3D-BASIS-ME (Tsopelas et al. 1994), whereas the effect of heating was recently coded in OpenSees (Kumar et al. 2015a, 2015b). However comprehensive models accounting for the static friction are still not used in practice. It must be recalled that the importance of the static friction was demonstrated in a numerical study by (Gandelli and Quaglini 2018) who used mechanical fuses to reproduce its contribution at the breakaway within the OpenSees framework.

A novel FPS isolator element provided with an enhanced friction model that incorporates the effects of axial load, velocity and heating, and includes new features such as the static coefficient of friction at the breakaway, was recently formulated in the object-oriented finite element Open Sees software by the Authors (Gandelli et al. 2019). After recalling the key features of the numerical code, the present study aims at presenting its application to the nonlinear analysis of a building, in order to demonstrate the advantages of the new FPS element and the expected enhancement in the prediction capability of the ensuing response history analysis.

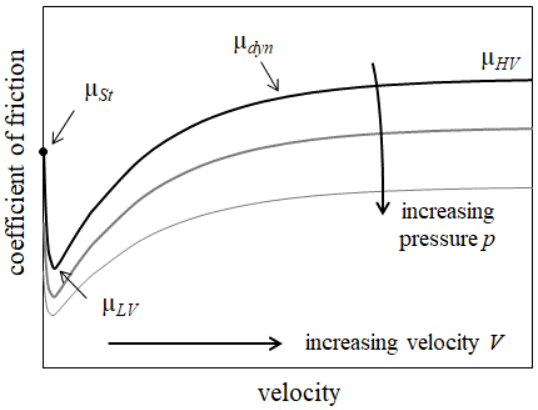

Figure 2. Typical variation of the coefficient of friction of thermoplastic materials with velocity and pressure

2 FINITE ELEMENT MODEL OF THE FPS

2.1 Physical model

A discrete element, labelled as *SingleFPSimple3d* element, is coded in the finite element software OpenSees to model a FPS with a single primary sliding surface and an articulated slider, like the example in Figure 1. The element has two nodes and twelve degrees of freedom: the first node (*i*-Node) is placed at the centre of the primary sliding surface and the second node (*j*-Node) at the centre of the secondary surface, with degrees of freedom in the global and the local coordinate systems defined as shown in Figure 3(a). The bearing can displace in six directions, namely, translate in the vertical and in two horizontal directions, twist about the vertical axis, and rotate about two horizontal axes. In the vertical direction, the slider is considered rigid, but the displacement in the horizontal direction induces the vertical rigid-body motion of the slider.

The response of the bearing is formulated by introducing the basic coordinate system represented in Figure 3(b), where the basic *x*-axis connects the centres of curvature of the sliding surfaces (C_i- and C_j-points, respectively), and the basic *y*- and *z*-axes follow the right-hand rule. In basic representation, the bearing has six degrees of freedom corresponding to as many displacements and rotations between the auxiliary C_i- and C_j-Nodes, and the force – deformation response is formulated by assuming that the auxiliary nodes are connected by six springs that represent the mechanical behaviour in the basic directions of the element: Axial, Shear 1, Shear 2, Torsion, Rotation1, and Rotation2.

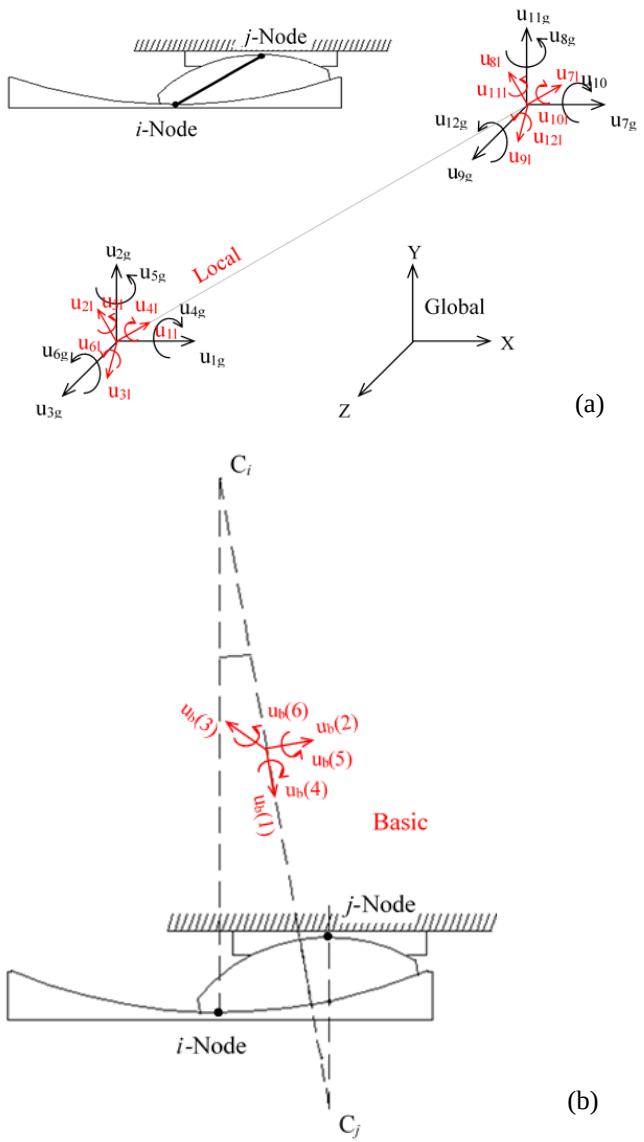

Figure 3. Coordinate systems of the FPS element in OpenSees: (a) global and local systems; (b) basic system

In the basic representation the general expressions of the element stiffness matrix is:

$$\left[K_b\right]=\begin{bmatrix} Axial & 0 & 0 & 0 & 0 & 0 \\ 0 & Shear1 & Shear21 & 0 & 0 & 0 \\ 0 & Shear12 & Shear2 & 0 & 0 & 0 \\ 0 & 0 & 0 & Torsion & 0 & 0 \\ 0 & 0 & 0 & 0 & Rotation1 & 0 \\ 0 & 0 & 0 & 0 & 0 & Rotation2 \end{bmatrix} \quad (1)$$

The element has coupled friction properties and post-yield stiffening due to the concave primary surface for the shear deformation, and linear elastic force–deformation relationships in the remaining four directions (to capture the uplift behaviour of the bearing, the elastic material model in the axial direction is modified for no-tension behaviour). Coupling between vertical and horizontal directions and between vertical direction and rotation is indirectly accounted for by consideration of geometric nonlinearity due to large displacement effects (Ray 2013). By default, P-Delta moments are entirely transferred to the primary sliding surface, so that rotations of the primary surface affect the shear behaviour of the bearing.

2.2 Numerical formulation

The force, displacement, and stiffness matrices are formulated at the component level in the basic coordinate system of the element, and transformation matrices are used to switch from basic to local and then from local to global coordinates. In the global system the contribution of each element is assembled to obtain the equations for the whole model, which are solved to obtain nodal forces and displacements. The nodal response quantities calculated in the global system are then transformed back to the element's local and basic coordinate systems to obtain forces and displacements in each element. The symbols $\{u_b\}$ and $\{\dot{u}_b\}$ are used hereinafter for the nodal displacement and nodal velocity vectors, while subscripts *b* and *l* designate the quantities in basic and local coordinates, respectively.

The hysteretic force–displacement relationship of the FPS in Shear1 and Shear2 directions is modelled according to the theory of plasticity, e.g. (Mosqueda et al. 2004), (Simo et Hughes 1998), while for the other basic directions the standard *UniaxialMaterial* elastic model is adopted. The procedure for calculation of the two shear forces (Gandelli et al. 2019) is recalled hereinafter.

At the first step, the effective radius in the two basic shear directions is calculated accounting for the deformation of the bearing element:

$$R_y=\sqrt{R^2-\left(u_b(3)\right)^2}$$
$$R_z=\sqrt{R^2-\left(u_b(2)\right)^2} \quad (2)$$

where R is the radius of curvature of the primary surface, and $u_b(2)$ and $u_b(3)$ are the displacements in the basic *y*- and *z*-directions defined in Figure 3(b). Noting that for small incremental displacements both vectors $\{u_b\}$ and $\{\dot{u}_b\}$ are tangential to the curved sliding surface, the absolute velocity is calculated as:

$$\left|\dot{u}_b\right|=\sqrt{\left(\dot{u}_b(2)\cdot\frac{u_b(2)}{R_y}+\dot{u}_b(3)\cdot\frac{u_b(3)}{R_z}\right)^2+\left(\dot{u}_b(2)\right)^2+\left(\dot{u}_b(3)\right)^2} \quad (3)$$

An iterative procedure is performed to calculate shear forces and stiffnesses.

At each iteration step, the normal force is calculated

$$N = -q_b(1) + q_{b,Old}(2)\cdot\frac{u_b(2)}{R_y} + q_{b,Old}(3)\cdot\frac{u_b(3)}{R_z} - q_{b,Old}(2)\cdot u_l(6) + q_{b,Old}(3)\cdot u_l(5) \quad (4)$$

where $q_b(1)$ is the axial force associated through the elastic *UniaxialMaterial* model to displacement $u_b(1)$ in Axial direction, and $q_{b,Old}(2)$ and $q_{b,Old}(3)$ are the shear forces in Shear1 and Shear2 directions calculated at the previous iteration. According to the adopted plasticity model, the total force along either shear direction has an elastic and a hysteretic force component, as shown in Figure 4. The stiffness $K2$ associated to the elastic component is given by the ratio between the normal force and the effective radius

$$K2_y = \frac{N}{R_y} \qquad K2_z = \frac{N}{R_z} \quad (5)$$

while the initial stiffness of the hysteretic component is given by the difference between the (isotropic) initial stiffness of the isolator, $K1$, and the elastic stiffness $K2$

$$K0_y = K1 - K2_y \qquad K0_z = K1 - K2_z \quad (6)$$

The displacements of the hysteretic component are used as a state variable for the plasticity model, and the trial values of the hysteretic shear forces $q_{Trial}(2)$ and $q_{Trial}(3)$ are calculated as:

$$qTrial(2) = K0_y\cdot\left(u_b(2) - u_{b,Pl\_Old}(2)\right)$$
$$qTrial(3) = K0_z\cdot\left(u_b(3) - u_{b,Pl\_Old}(3)\right) \quad (7)$$

where $u_{b,Pl\_Old}(2)$ and $u_{b,Pl\_Old}(3)$ are the plastic displacements at the previous iteration.

Since FPS isolators with conventional spherical surfaces exhibit isotropic behavior for bidirectional motion, a circular yield condition is adopted. A dummy parameter Y is introduced to regulate the transition from the elastic to the plastic regime, accounting for the change of the FPS from sticking to sliding behaviour:

$$Y = |qTrial| - q_{yield} \quad (8)$$

In Equation (8), q_{yield} is the yield force calculated in accordance with the assumed friction model and

$$|qTrial| = \sqrt{(qTrial(2))^2 + (qTrial(3))^2} \quad (9)$$

is the resultant hysteretic shear force.

When $Y \leq 0$, the element performs an elastic step and the shear forces are calculated as

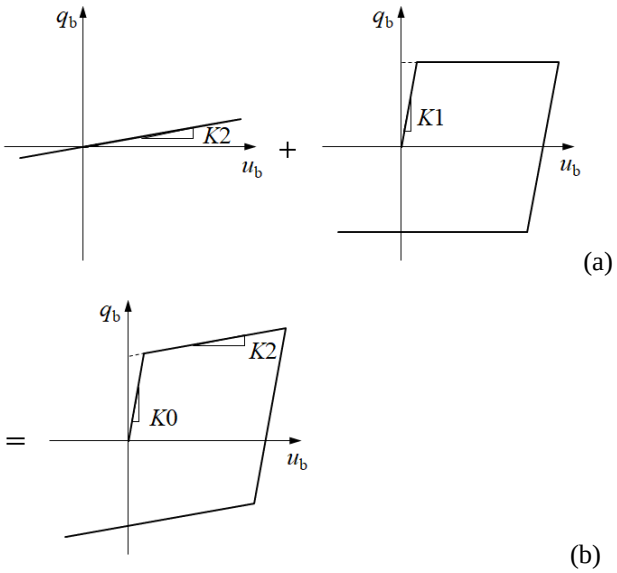

Figure 4: Elastic and hysteretic resisting force components of the plasticity model (a), and resulting force – displacement relationship (b); from (Simo and Huges 1999)

$$q_b(2) = qTrial(2) + K2_y\cdot u_b(2) - N\cdot u_l(6)$$
$$q_b(3) = qTrial(3) + K2_z\cdot u_b(3) + N\cdot u_l(5) \quad (10)$$

and the tangent stiffness for the coupled shear directions is

$$K_b(2,2) = K_b(3,3) = K1$$
$$K_b(2,3) = K_b(3,2) = 0 \quad (11)$$

When $Y > 0$ plasticity is activated and the software performs a return mapping algorithm to calculate the resisting force. By assuming an associative plastic flow rule, the trial slip in either shear direction is obtained by dividing the dummy parameter Y by the initial elastic stiffness of the hysteretic component

$$dGamma_y = Y / K0_y$$
$$dGamma_z = Y / K0_z \quad (12)$$

and the plastic displacement is updated

$$u_{b,Pl}(2) = u_{b,Pl\_Old}(2) + dGamma_y\cdot\frac{qTrial(2)}{|qTrial|}$$
$$u_{b,Pl}(3) = u_{b,Pl\_Old}(3) + dGamma_z\cdot\frac{qTrial(3)}{|qTrial|} \quad (13)$$

Eventually the shear forces and the associated components of the tangent stiffness are calculated:

$$q_b(2) = q_{yield}\cdot\frac{qTrial(2)}{|qTrial|} + K2_y\cdot u_b(2) - N\cdot u_l(6)$$
$$q_b(3) = q_{yield}\cdot\frac{qTrial(3)}{|qTrial|} + K2_z\cdot u_b(3) + N\cdot u_l(5) \quad (14)$$

$$K_b(2,2) = K0_y \cdot q_{yield} \frac{qTrial(3) \cdot qTrial(3)}{|qTrial|^3} - K2_y$$

$$K_b(3,3) = K0_z \cdot q_{yield} \frac{qTrial(2) \cdot qTrial(2)}{|qTrial|^3} - K2_z$$

$$K_b(2,3) = -K0_z \cdot q_{yield} \frac{qTrial(2) \cdot qTrial(3)}{|qTrial|^3} \quad (15)$$

$$K_b(3,2) = -K0_y \cdot q_{yield} \frac{qTrial(2) \cdot qTrial(3)}{|qTrial|^3}$$

The procedure is run iteratively until convergence is achieved. The resulting shear force components are used to formulate the element stiffness matrix in the basic system [K_b] according to Equation (15). The element stiffness matrix is then transformed into the local coordinate system and "P-Delta" and "V-Delta" moment stiffness terms are added to the local force vector. The local stiffness matrix is finally transformed into the global coordinate system and assembled to the contributions of the other elements to obtain the system of equations governing the response of the overall model.

2.3 Friction model

The standard *SingleFPSimple3d* element calculates the yield force based on the friction law coded in the associated *FrictionModel* command. Different friction models are available in OpenSees, to define the coefficient of friction either as a constant (Coulomb friction) or as a function of the sliding velocity, of the axial load, or of both of them.

The novel element (Gandelli et al. 2019), called the *CSSBearing_BVNC* element, has been implemented by modifying the source code of the standard element in order to account for two distinct plastic material models:

$$q_{yield} = \mu_B \cdot N \quad \text{for} \quad h < 1$$
$$q_{yield} = \mu_{VNC} \cdot N \quad \text{for} \quad h \geq 1 \quad (16)$$

where h is a counter that is updated each time the condition $Y > 0$ occurs. At the beginning of the analysis the counter is initialized ($h = 0$), and the yield force q_{yield} is defined by a circular yield criterion according to a Coulomb material, i.e. $q_{yield} = \mu_B \cdot N$, where μ_B is the static coefficient of friction at breakaway. When the yield condition $Y = 0$ is achieved for the first time, the variable h is upgraded to $h = 1$, and from this time on the plasticity algorithm switches to the user-defined *VNC_Friction* material model. This material model calculates the yield force as $q_{yield} = \mu_{VNC} \cdot N$, with μ_{VNC} defined as

$$\mu(N,V,c) = f_{NV}(N,V) \cdot f_c(c) \quad (17)$$

Here $f_{NV}(N, V)$ is a function that accounts for the effects of the instantaneous values of axial load N and velocity V, and $f_c(c)$ is a second function that incorporates for the effect of the cumulated heat flux at the sliding surface through the degradation variable c.

For the function $f_{NV}(N, V)$ the exponential formulation (Constantinou et al. 1990) is assumed

$$f_{NV}(N,V) = \mu_{HV}(N) - [\mu_{HV}(N) - \mu_{LV}(N)] \cdot \exp(-\alpha|\dot{u}_b|) \quad (18)$$

where μ_{LV} and μ_{HV} are the values of the dynamic coefficient of friction at low velocity and high velocity, respectively, and α determines the rate of change of the dynamic coefficient of friction with the sliding velocity. The coefficients μ_{LV}, μ_{HV} and α depend on the instantaneous value of the axial load and are updated at each iteration according to power law expression (Bowden and Tabor 1964)

$$\mu_{HV}(N) = A_{HV} \cdot N^{(n_{HV}-1)}$$
$$\mu_{LV}(N) = A_{LV} \cdot N^{(n_{LV}-1)} \quad (19)$$
$$\alpha(N) = \alpha_0 + \alpha_1 \cdot N + \alpha_2 \cdot N^2$$

with A_{LV}, $A_{HV} > 0$, n_{LV}, $n_{HV} \leq 1$ and α_0, α_1, $\alpha_2 > 0$.

The effect of heating on the coefficient of friction is considered by means of the degradation function f_c (Lomiento et al. 2013):

$$f_c(c) = \exp\left[-\left(c / c_{ref}\right)^{\gamma}\right] \quad (20)$$

where c_{ref} is a parameter that regulates the rate of degradation (the smaller c_{ref}, the higher the degradation), γ is a parameter that controls the shape of the function, and c is a variable that depends on the total power dissipated at the sliding surface and the distance travelled by the slider (Gandelli et al. 2019):

$$c = \int_0^t N \cdot |\dot{u}_b|^2 \, dt \quad (21)$$

At each time step, the increment Δc of the variable over the time interval Δt is calculated by numerical integration of Equation (20), and used to updated the variable as $c(t + \Delta t) = c(t) + \Delta c$.

Ten parameters are used in the implementation of the *CSSBearing_BVNC* element, namely μ_B (static or breakaway coefficient of friction), A_{LV}, A_{HV}, n_{LV}, n_{HV} (load-effect parameters), α_0, α_1, and α_2 (velocity-effect parameters), and c_{ref} and γ (degradation-effect parameters). The novel model

encompasses standard friction models coded in OpenSees libraries, such as *Coulomb*, *VelDependent*, and *VelNormalFrcDep* models, which can be obtained as special cases by setting the relevant parameters as shown in Table 1.

Table 1. Conventional *FrictionModel* objects coded in OpenSees encompassed by the *CSSBearing_BVNC* element and relevant parameters (other parameters are arbitrary).

OpenSees model	Parameters
VelNormalFrcDep	$\mu_B = A_{LV}$
	$c_{ref} = 10^{100}$, $\gamma = 1$
VelDependent	$\mu_{St} = A_{LV}$
	$n_{LV} = n_{HV} = 1$
	$c_{ref} = 10^{100}$, $\gamma = 1$
Coulomb	$A_{LV} = A_{HV} = \mu_{St}$
	$n_{LV} = n_{HV} = 1$
	$\alpha_0 = 10^{100}$, $\alpha_1 = \alpha_2 = 0$
	$c_{ref} = 10^{100}$, $\gamma = 1$

2.4 *Code verification*

Code-to-code comparison with the conventional *SingleFPSimple3d* element was performed to verify the correct implementation of the static coefficient of friction and the heat degradation of the dynamic coefficient of friction in the new element.

A simple SDOF model, with a 100 tons lumped mass producing a vertical force N = 981 kN and connected to ground by an FPS isolator element, is considered for the analyses. The isolator has an effective radius R = 3500 mm and initial elastic stiffness $K1$ = 2.803 kN/m. An unidirectional sinusoidal acceleration with amplitude 0.40 g and period 1.0 s is applied at ground level. No damping is assigned to the system.

Model parameters are assigned to the *CSSBearing_BVNC* element as follows: μ_B = 0.30 $(10^{-3}$ kN$)^{-1}$, A_{LV} = 0.05 $(10^{-3}$ kN$)^{-1}$, A_{HV} = 0.15 $(10^{-3}$ kN$)^{-1}$, $n_{LV} = n_{HV}$ = 1, α_0 = 0.05 s/mm, $\alpha_1 = \alpha_2 = 0$, $c_{ref} = 5\times10^{15}$ $(10^{-3}$ N$)$ mm^2/s and γ = 1.0. The calculated force – displacement loop and the response time histories are illustrated in Figure 5. The breakaway force of 297 kN matches the theoretical value of 300 kN (0.30 · 1000 kN); the force history is smooth, with no spikes at the motion reversals though here the sliding velocity is zero, demonstrating the correct switch of the yield condition from μ_B to μ_{VNC} after the breakaway.The degradation of the coefficient of friction is evident from the comparison of the shear force calculated by the *CSSBearing_BVNC* element to the force calculated using the *SingleFPSimple3d* element with "*VelDependent*" friction model and assigned parameters A_{LV} = 0.05 $(10^{-3}$ kN$)^{-1}$, A_{HV} = 0.15 $(10^{-3}$ kN$)^{-1}$ and α = 0.05 s/mm: the difference is on the order of -5.5% at the first cycle, and -28.5% at the tenth cycle. Figure 6 compares the coefficient of friction predicted at peak velocity from the software (red dots) to the expected value f_{NV} f_c (solid line), where the reductive factor f_c is analytically calculated in accordance with Equations (19) and (20), showing that the deviation is less than 0.01.

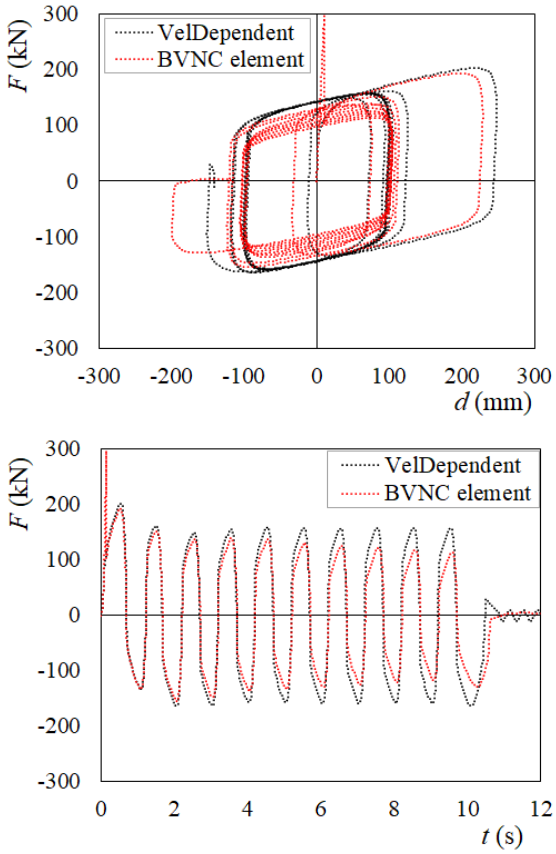

Figure 5: Code-to-code comparison between *CSSBearing_BVNC* element and standard element with assigned *VelDependent* friction model

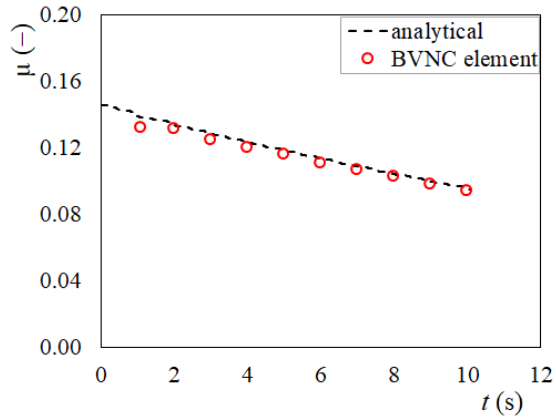

Figure 6: Degradation of coefficient of friction predicted by the *CSSBearing_BVNC* element compared to the analytical solution

3 TIME HISTORY ANALYSES

To evaluate the performance of the *CSSBearing_BNVC* code in a practical application, dynamic analyses of a multi-degrees-of-freedom structure have been performed in accordance with the provisions of the Italian Building Code (CSLLPP 2018), and the results compared to the prediction of the standard *SingleFPSimple3d* element. The study addresses the effect of the static coefficient of friction, while the heating effect is dealt with in another publication, e.g. (Gandelli et al. 2019).

3.1 Case study

A regular reinforced concrete, moment-resisting-frame building is considered. The structure has a double symmetric square plan of 18 by 18 m with three bays of 6 m in both horizontal directions, and four stores at 3 m each, for a total height of 12 m, and is supported from a rigid base slab (Figure 7). Rectangular (300×300 mm) beams are used at every floor. The columns have square cross-section, with dimensions of 500×500 mm at ground and first floor, and 400×400 mm at second and third floors. Seismic masses were evaluated by taking into account the full permanent loads plus 30% of the live loads for residential buildings (CSLLPP 2018). The seismic weight of the floors and the base slab is 2400 kN each, resulting in a cumulative weight of the building of 12000 kN.

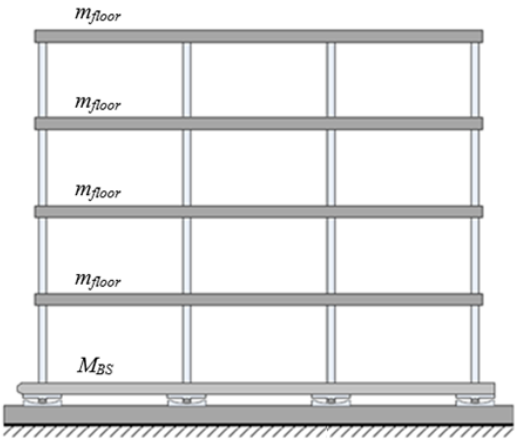

Figure 7: Section of the case-study base-isolated building; m_{floor} is the mass of each floor and M_{BS} is the mass of the base slab

The structural model is implemented in the OpenSees v.2.5.4 software. The base-isolated superstructure is formulated as an elastic system in accordance with the provisions of the Italian Building Code (CSLLPP 2018). A moment-resisting frame structure with rigid joints is assumed, and *ElasticBeamColumn* elements are used to model both horizontal and vertical members. The bending stiffness assigned to the columns is Kc = 69.131 kN/mm for the 500×500 mm columns, and Kc' = 31.067 kN/mm for the 400×400 mm columns, respectively, while a *RigidFloorDiaphragm* multi-points constraint is introduced at each story to account for the in-plane stiffness of the floor slabs. The fundamental period of the superstructure is T_{SS} = 0.31 s. Stiffness proportional structural damping (Ryan and Polanco 2008) is considered, with parameters assigned to achieve 5% damping ratio at a 3.5 s period.

3.2 Isolation system

The isolation system consists of sixteen FPS isolators, with effective radius R = 2500 mm, corresponding to a design period $Tiso$ = 3.17 s, placed at the foundation level, one bearing underneath each column. The initial stiffness of the bearings is 479.52 kN/mm. The *CSSBearing_BNVC* element is used to model the isolators and the parameters of the friction model for its implementation are given in Table 2, where a ratio $\mu_B / \mu_{LV} = 4$ is assumed. For simplicity, the effects of the vertical load and heating on the coefficient of friction are disregarded.

Table 2. Parameters of the friction model assigned in the case study.

Parameter	Unit	Value
μ_B	-	0.12
A_{LV}	$\left(10^{-3}\ \text{N}\right)^{(1-n_{LV})}$	0.030
A_{HV}	$\left(10^{-3}\ \text{N}\right)^{(1-n_{HV})}$	0.075
n_{LV}	-	1
n_{HV}	-	1
α_0	s mm^{-1}	0.055
α_1	s mm^{-1} N^{-1}	0
α_2	s mm^{-1} N^{-2}	0
c_{ref}	(10^{-3} N) mm^2/s	10^{100}
γ	–	1

Baseline references for comparison are derived from nonlinear analyses performed by using the *SingleFPSimple3d* element with *VelDependent* FrictionMaterial and assigned parameters μ_{LV} = 0.03, μ_{HV} = 0.075, and α = 0.055 s/mm.

3.3 Seismic input

Nonlinear analyses of the isolated building are performed assuming an ordinary structure

(functional class II) with nominal life of 50 years, corresponding to a reference period of 50 years, located in Naples, South Italy (14.28° longitude, 40.86° latitude), topographic category T1, soil type A (rock or other rock-like geological formation). Target elastic spectra were determined in accordance with the provisions of the Italian Building Code for Damage Limitation (SLD) and Human Life Saveguard (SLV) earthquake hazard levels.

For either hazard level, a set of 21 independent bidirectional ground motions was selected with REXEL v3.4 beta (Iervolino et al. 2010) software from the European Strong-motion Database (Ambraseys et al, 2002). The magnitude (Mw) of the ground motions was chosen within the interval (5–8), and the epicentral distance (Rep) in the range (0–50 km), and more precisely 7 accelerograms with Rep in the range (0–10 km), 7 accerelograms with Rep in the range (10–20 km), and 7 accerelograms with Rep in the range (20–50 km). The selected waveforms were scaled to the design Peak Ground Acceleration level of either 0.059 g (SLD level) or 0.168 g (SLV level) calculated according to the Code. At either limit state, the average spectrum of the set of accelerograms matches the Italian Building Code spectrum within -10/+30% tolerance in the period range 0.15 – 4.0 sec.

3.4 Results

The analyses showed that weak or moderate intensity ground motions may fail to trigger the FPS isolators when the static coefficient of friction is considered. Sliding of the FPS takes place when the shear force through the bearing, which is the resultant of the inertial forces acting on the superstructure, exceeds the frictional resisting force at the sliding surface. At SLD level, by considering the contribution of the static friction, 18 out of the 21 selected ground motions failed to promote sliding (Table 3); on the contrary at SLV sliding of the bearings always occurred.

Table 3. Number of accelerograms triggering the FPS isolators calculated by either *BVNC* and *VelDependent* friction models.

Friction model	Hazard level	Events
BVNC	SLD	3
	SLV	21
VelDependent	SLD	21
	SLV	21

The response of the structure was appraised through the following quantities: (i) the horizontal displacement of the base slab d_{iso}; (ii) the ratio between the toal shear force V_{iso} through the FPS isolators and the total vertical load (N_{SS} + N_{BS}), where N_{SS} and N_{BS} are the seismic weights of the superstructure and the base slab; (iii) the inter-story drift (Δ); (iv) the superstructure seismic coefficient (*SC*) defined as the ratio between the column shear and the supported seismic weight; (v), the maximum floor acceleration in the superstructure a_{SS}. The results are summarized in Figure 8, in terms of the mean values for each set of ground motions.

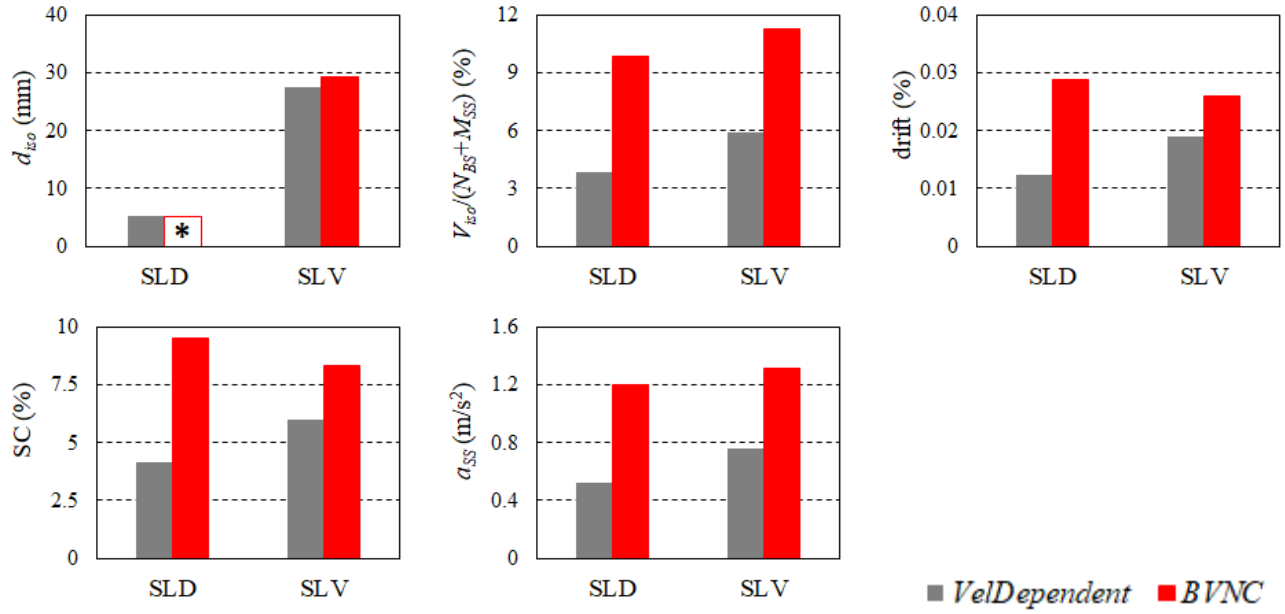

Figure 8: Response of the base-isolated structure at SLD and SLV hazard levels

The improved accuracy of the analyses introduced by the C*SSBearing_BNVC* element is discussed hereinafter by comparison with the results provided by the *SingleFPSimple3d* element with *VelDependent* friction model.

The effect of the static friction on the maximum displacement seems to be negligible at SLV level, with only a +6% increase over the baseline result; this is explained by considering that small movements which may occur at the beginning of the shake, before the occurrence of the peak displacement, are prevented. At SLD a direct comparison of the displacement demand is not feasible because of the large number of ground motions which failed to trigger the isolators.

The effect of static friction on the shear force through the FPS is shown in the second panel of Figure 8, with a +155% increase at SLD and a +91% increase at SLV over the baseline values. By recalling that the peak displacement is not significantly affected from the static friction, the rise in force is essentially due to the frictional force at the breakaway. It must be noted that the average shear force predicted at SLD by the C*SSBearing_BNVC* element is 66% higher than the value calculated at SLV by the standard element, and very close (only 13% less) to the shear force at SLV according to the new element.

In the event the FPS isolators are not triggered, the superstructure behaves as a fixed base structure, experiencing higher accelerations than expected according to the design of the isolation system. This is evident from the analyses relevant to the SLD level, which demonstrate +128% increase in peak floor acceleration, +130% increase in shear force in the most stressed columns, and +134% increase in inter-story drift over the baseline values. The internal forces and deformations of the superstructure at SLD are larger than the values predicted by the standard element at SLV: +53% for drift, and + 59% for both column shear and floor acceleration. Although for the case study the inter-story drifts are within the serviceability limits (CSLLPP 2018), attention is drawn to the possible consequences of large drifts and floor accelerations on the performance of nonstructural elements.

At SLV level, accounting for the static friction at breakaway provide higher values in superstructure drift (+38%), column shear (+40%), and floor acceleration (+73%) when compared to the response predicted through the *VelDependent* friction model, though the deviation is smaller than at SLD level.

4 CONCLUSIONS

A novel *CSSBearing_BVNC* element has been formulated in OpenSees software by modifying the standard *SingleFPSimple3d* element to introduce new features such as the static coefficient of friction at the breakaway and the degradation of the coefficient of friction due to heating.

A comparative evaluation performed through a case study highlights the potential of the newly developed isolator element to yield a more accurate estimation when applied to real situations, with a +40% increase in estimate of superstructure drift and column shear force at Human Life Safeguard hazard level, and identification of possible non-sliding of the isolators under weak or medium intensity earthquakes at Damage Prevention level. Since current FPS finite elements coded in software programs for structural analysis do no incorporate the static coefficient of friction, the analyses may underestimate the forces and accelerations induced in the superstructure, especially in cases where the static coefficient of friction is significantly higher than the low-velocity coefficient μ_{LV}. The proposed *CSSBearing_BVNC* element is expected to overcome this issue.

REFERENCES

Ambraseys, N., Smit, P., Sigbjornsson, R., Suhadolc, P., Margaris, B. 2002. *Internet-Site for European Strong-Motion Data. European Commission*, Research-Directorate General, Environment and Climate Programme, http://www.isesd.cv.ic.ac.uk/ESD/2.

Barone, S, Calvi, G.M., Pavese, A. 2017. Experimental dynamic response of spherical friction-based isolation devices. *Journal of Earthquake Engineering*, DOI: 10.1080/13632469.2017.1387201.

Bowden, F.P., Tabor, D. 1964. *The friction and lubrication of solids – part II.* Oxford University Press.

Campbell, T.I., Fatemi, M.J., Manning, D.G. 1993. Friction in bridge bearings with contaminated TFE slide surface. *ASCE Journal of Structural Engineering*, **119**(11), 3169-3177.

Constantinou, M.C., Tsopelas, P., Kasalanti, A., Wolff, E.D. 1999. *Property modification factors for seismic isolation bearings. Report No. MCEER-99-0012*. Multidisciplinary Center for Earthquake Engineering Research.

Constantinou, M.C., Mokha, A., Reinhorn, A. 1990. Teflon bearings in base isolation II: modelling. *ASCE Journal of Structural Engineering*, **116**(2), 455-474.

Constantinou, M.C., Whittaker, A.S., Kalpakidis, Y., Fenz, D.M., Warn, G.P. 2007. *Performance of seismic isolation hardware under service and seismic loading. Report*

MCEER-07-0012. Multidisciplinary Center for Earthquake Engineering Research.

CSI 2016. *Analysis Reference Manual for SAP2000®, ETABS®, SAFE® and CSiBridge*. Computers and Structures Incorporated.

CSLLPP 2018. *D.M. 22.03.2018, Norme Tecniche per le Costruzioni*, Consiglio Superiore dei Lavori Pubblici (in Italian).

Dolce, M., Cardone, D., Croatto, F. 2005. Frictional behavior of steel-PTFE interfaces for seismic isolation. *Bulletin of Earthquake Engineering*, **3**(1), 75-99.

Fenz, D.M., Constantinou, M.C. 2006. Behaviour of the double concave Friction Pendulum bearing. *Earthquake Engineering and Structural Dynamics*, **35**(11), 1403–1424.

Gandelli, E., Penati, M., Quaglini, V., Lomiento, G., Miglio, E., Benzoni, G.M. 2019. A novel OpenSees element for single curved surface sliding isolators. *Soil Dynamics and Earthquake Engineering*, **119**, 433-453.

Gandelli, E., Quaglini, V. 2018. Effect of the static coefficient of friction of curved surface sliders on the response of an isolated building. *Journal of Earthquake Engineering*, DOI: 10.1080/13632469.2018.1467353.

Iervolino, I., Galasso, C., Cosenza, E. 2010. REXEL: computer aided record selection for code-based seismic structural analysis. *Bulletin of Earthquake Engineering*, **8**(2), 339–362.

Kumar, M., Whittaker, A.S., Constantinou, M.C. 2015. Characterizing friction in sliding isolation bearings. *Earthquake Engineering and Structural Dynamics*, **44**(9), 1409-1425.

Kumar, M., Whittaker, A.S., Constantinou, M.C. 2015. *Seismic isolation of nuclear power plants using sliding bearings. Report MCEER-15-0006*. Multidisciplinary Center for Earthquake Engineering Research.

Lomiento, G., Bonessio, N., Benzoni, G.M. 2013. Friction Model for sliding bearings under seismic excitation. *Journal of Earthquake Engineering*, **17**(8), 1162-1191.

McKenna, F., Fenves, G., Scott, M., 2006. *Computer program OpenSees: open system for earthquake engineering simulation*, Pacific Earthquake Engineering Research Center.

Mokha, A.S., Constantinou, M.C, Reinhorn, A.M. 1991. Experimental study of friction-pendulum isolation system. *ASCE Journal of Structural Engineering*, **117**(4), 1201-1217.

Mosqueda, G., Whittaker, A.S., Fenves, G.L., Mahin, S.A. 2004. *Experimental and analytical studies of the Friction Pendulum system for the seismic protection of bridges, Report No. UCB/EERC-2004/01*. Pacific Earthquake Engineering Research Center.

Quaglini, V., Dubini, P., Ferroni, D., Poggi, C. 2009. Influence of counterface roughness on friction properties of engineering plastics for bearing applications. *Materials and Design*, **30**(5), 1650–1658.

Quaglini, V., Dubini, P., Poggi, C. 2012. Experimental assessment of sliding materials for seismic isolation systems. *Bulletin of Earthquake Engineering*, **10**(2), 717–740.

Quaglini, V., Bocciarelli, M., Gandelli, E., Dubini, P. 2014. Numerical assessment of frictional heating in sliding bearings for seismic isolation. *Journal of Earthquake Engineering*, **18**(8), 1198–1216.

Ray, T. 2013. *Modeling of multi-dimensional inelastic and nonlinear elastic structural systems.* PhD dissertation, State University of New York at Buffalo.

Ryan, K.L., Polanco, J. 2008. Problems with Rayleigh damping in base-isolated buildings. *ASCE Journal of Structural Engineering*, **134**(11), 1780-1784.

Sarlis, A.A., Constantinou, M.C., Reinhorn, A.M. 2013. *Shake table testing of Triple Friction Pendulum Isolators under extreme conditions. Report No. NCEER-13-0011*. National Center for Earthquake Engineering Research.

Simo, J.C., Hughes, T.J.R. 1998. *Computational inelasticity*. Springer.

Tsopelas, P.C., Constantinou, M.C., Reinhorn, A.M. 1994. *3D-BASIS-ME: Computer program for nonlinear dynamic analysis of seismically isolated single and multiple structures and liquid storage tanks. Report NCEER-94-0010.* National Center for Earthquake Engineering Research.

Zayas, V.A., Low, S.S., Mahin, S.A. 1987. *The FPS earthquake protection system. Report No. 87-01*. Earthquake Engineering Research Cente.

Zayas, V.A., Low, S.S., Mahin, S.A. 1990 A simple pendulum technique for achieving seismic isolation. *Earthquake Spectra*, **6**(2), 317-333.